Carolina Moilanen*, Tomas Björkqvist, Markus Ovaska, Juha Koivisto, Amandine Miksic, Birgitta A. Engberg, Lauri I. Salminen, Pentti Saarenrinne and Mikko Alava

Influence of strain rate, temperature and fatigue on the radial compression behaviour of Norway spruce

DOI 10.1515/hf-2016-0144
Received September 8, 2016; accepted March 1, 2017; previously published online xx

Abstract: A dynamic elastoplastic compression model of Norway spruce for virtual computer optimization of mechanical pulping processes was developed. The empirical wood behaviour was fitted to a Voigt-Kelvin material model, which is based on quasi static compression and high strain rate compression tests (QSCT and HSRT, respectively) of wood at room temperature and at high temperature (80–100°C). The effect of wood fatigue was also included in the model. Wood compression stress-strain curves have an initial linear elastic region, a plateau region and a densification region. The latter was not reached in the HSRT. Earlywood (EW) and latewood (LW) contributions were considered separately. In the radial direction, the wood structure is layered and can well be modelled by serially loaded layers. The EW model was a two part linear model and the LW was modelled by a linear model, both with a strain rate dependent term. The model corresponds well to the measured values and this is the first compression model for EW and LW that is based on experiments under conditions close to those used in mechanical pulping.

***Corresponding author: Carolina Moilanen,** Mechanical Engineering and Industrial Systems, Tampere University of Technology, P.O. Box 589, FI-33101, Tampere, Finland, Phone: +358-40-198-1599, e-mail: carolina.moilanen@tut.fi
Tomas Björkqvist: Automation and Hydraulic Engineering, Tampere University of Technology, P.O. Box 692, FI-33101, Tampere, Finland
Markus Ovaska, Juha Koivisto, Amandine Miksic and Mikko Alava: Department of Applied Physics, School of Science, Aalto University, P.O. Box 11100, FI-00076, Aalto, Finland
Birgitta A. Engberg: Department of Chemical Engineering, Mid Sweden University, Holmgatan 10, SE-85170, Sundsvall, Sweden
Lauri I. Salminen: VTT, current at Andritz Oy, Askonkuja 9G, 15100 Lahti, Finland
Pentti Saarenrinne: Mechanical Engineering and Industrial Systems, Tampere University of Technology, P.O. Box 589, FI-33101, Tampere, Finland

Keywords: radial compression behaviour, dynamic modelling of defibration, earlywood, high strain rate test, latewood, moist Norway spruce, split-Hopkinson pressure bar, Voigt-Kelvin material model

Introduction

The basic principle in mechanical pulping is to separate and treat fibres by a series of shear and compression loadings. The process generates both internal and external fibrillation so that the pulp will be suitable for papermaking. In mechanical pulping, moist or wet wood is processed at elevated temperatures and at high strain rates. The resulting fibre material is used for paper and board products. The energy consumption in mechanical pulping is a burden. The energy consumption can be reduced by either altering the process or the raw material. Lower energy consumption is required to a given tensile index at elevated pressures/temperatures (Becker et al. 1977; Höglund et al. 1997; Fernando et al. 2011). Fernando et al. (2011) used a staining method to evaluate the delamination and internal fibrillation of the pulps and observed that these properties increased significantly at high temperature in combination with high consistency. A pressure of 2–4 bar caused no obvious damage to the fibre cross-section, while nano-cracks were found in fibres subjected to 6–12 bar and micro-cracks in fibres subjected to 14–18 bar (Xing et al. 2008). The refining steam pressure influences the sorption behaviour and surface properties of the fibre (Neimsuwan et al. 2008). Mechanical pre-treatment as a part of the chipping process has been presented by Isaksson et al. (2013), who performed an experimental and numerical study of different knife-edge angles and chip lengths, for a chip length of 25 mm and a friction coefficient of 0.3 at which, the optimal knife angle would be 54°. Chemical pre-treatments with cellulases (Lecourt et al. 2010) and oxalic acid (Li et al. 2011) reduce the energy consumption but they also affect the pulp quality.

Authenticated | carolina.moilanen@tut.fi author's copy
Download Date | 4/8/17 5:58 AM

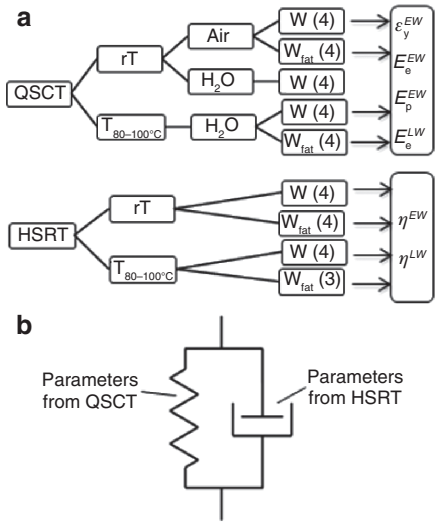

Figure 1: (a) Flow diagram showing the experimental design with quasi static compression tests (QSCT) and high strain rate compression tests (HSRT) at room temperature (rT) and 80°C–100°C ($T_{80–100°C}$) and tested in air and submerged in water (H_2O) with number of native (W) and pre-fatigued (W_{fat}) samples and links to the part of the Voigt-Kelvin material model proportional to strain (ε) and to the part proportional to strain rate ($\dot{\varepsilon}$) and (b) the schematic representation of the Voigt-Kelvin material model with links to the material testing.

The most common raw material for mechanical pulping in the Nordic countries is Norway spruce (*Pieca abies* (L.) H. Karst). In most softwoods, there is a distinct difference in fibre stiffness between the fibres that are formed in the spring (earlywood, EW) and later in the summer (latewood, LW). The fibres in EW have typically thin cell walls and large cell voids and are therefore soft. The fibres in LW have relatively thick cell walls and small cell voids. Here, the fibres are much stiffer than EW fibres. The compression stress-strain curve for average wood is dominated by EW and has three regions: an elastic region, a plateau region where a small stress increase gives a strong response in strain and a densification region (Salmén et al. 1997; Law et al. 2006).

Wood is softened significantly by increasing temperature. The plateau stress decreases linearly with increasing temperature from 25°C to 100°C at low strain rate (Uhmeier and Salmén 1996; Salmén et al. 1997). The plateau stress levels out at 130°C to 160°C, while the changes in the plateau stress above 160°C are caused by chemical changes (Salmén et al. 1997). The yield strain does not change at the interval 0°C to 100°C and the yield stress drops by one decade at the interval 0°C–200°C during quasi static radial compression (Uhmeier and Salmén 1996; Law et al. 2006). The yield strain is dependent on the structure and is therefore not temperature dependent as in the case of yield stress. Uhmeier et al. (1998) also observed thermal degradation between 150°C and 200°C. Thermal degradation at very high temperatures is not central for this study.

The strain rate is known to have an impact on the compression behaviour of wood. The moisture content (MC) affects the response at different strain rates. The difference in modulus of elasticity (MOE) between low and high strain rate compression is low for dry wood (W_{dry}) but more significant for water saturated wood (W_{sat}). In low strain rate compression, the MOE of W_{sat} is smaller than that of W_{dry}. At high strain rate, W_{sat} is sometimes stiffer than W_{dry} due to the different behaviour of the liquid in the cell voids. The liquid could flow out with less resistance during compression at low strain rate than at high strain rate (Renaud et al. 1996). Pulp raw material has moderate MC and therefore, the focus of this study is on cell wall properties at fibre saturation level.

Material fatigue is the weakening of a material caused by cyclic or repeated loading. Higher temperature and lower frequency favours the structural breakdown of wood (Salmén 1987; Salmén et al. 1985). The fatigue damage accumulation starts with crack initiation, proceeds with micro crack formation and ends up in macro crack formation (Hamad and Provan 1995). A layer of fatigued wood fibres is generated during grinding (Salmi et al. 2011). A combined shear and compression load followed by pure compression is more beneficial than pure repeated compression, when aiming at a large deformation and low energy consumption (De Magistris 2005). A pre-fatigue treatment of the raw material reduces the specific energy consumption in grinding (Salmi et al. 2012a). Fatigue treatment reduces the MOE to one third compared with native wood at both 20°C and 135°C (Moilanen et al. 2016).

The models can be divided into micromechanical models focusing on details of the wood structure and continuum models dealing with the overall behaviour. For the application in mechanical pulping, the fatigue development is more important than the micromechanical compression behaviour. For this reason, detailed micromechanical models are not necessary and a simpler model is sufficient. Adalian and Morlier (2001) compared their wood model based on the hypo elastic law with a classic elastoplastic model and found the simulation results of the former more realistic than the results of the latter. Björkqvist (2002) and Björkqvist et al. (1999) modelled wood as a simple, linear Voigt-Kelvin solid for simulations and optimization of the deformation and temperature development behind the fatigue work in the course of a grinding process. Hanhijärvi and Mackenzie-Helnwein (2003) developed a two-dimensional (2D) model that defines a decomposition of the total strain into the sum of several strain tensors associated with different deformation mechanisms. All existing continuum models have some problems for the application to larger

Authenticated | carolina.moilanen@tut.fi author's copy
Download Date | 4/8/17 5:58 AM

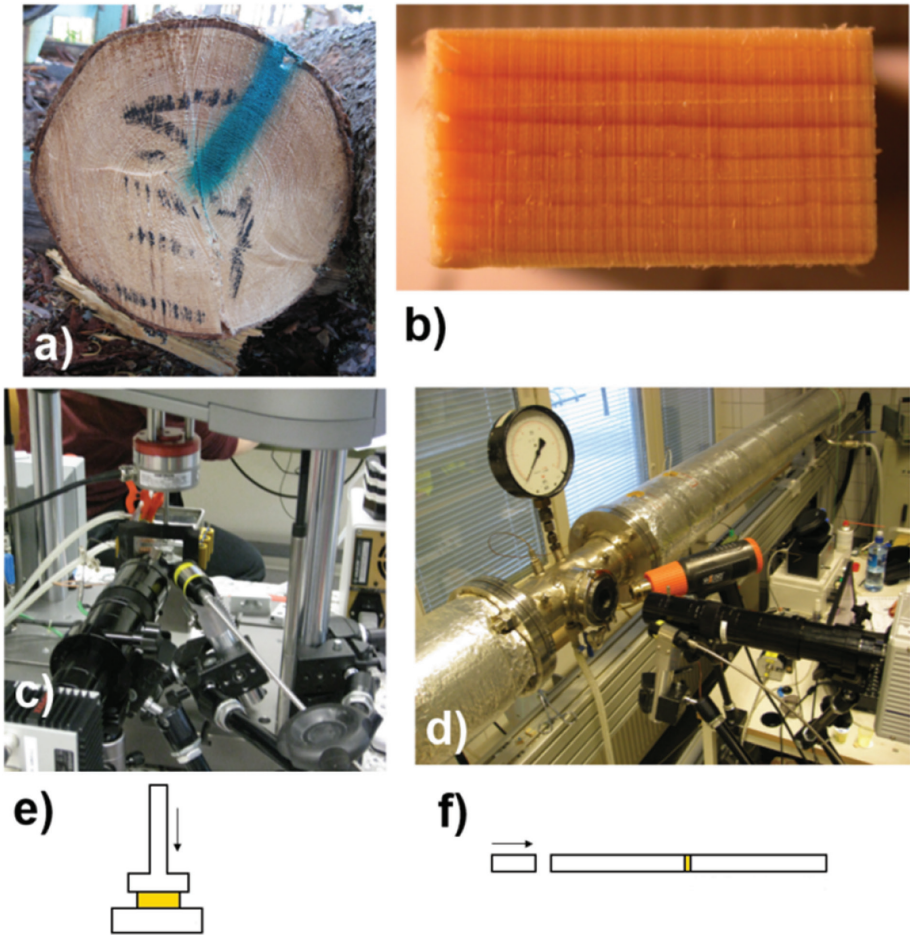

Figure 2: Images of (a) raw material, (b) sample for high strain rate testing, (c) measurement setup with Instron E1000 tensile testing machine for quasi static testing (QSCT), (d) measurement setup with the encapsulated split-Hopkinson for HSRT, (e) schematic sketch of the QSCT where the arrow indicates the movement of the piston and (f) schematic sketch of the HSRT where the arrow indicates the movement of the striker.

simulations of the mechanical pulping. Therefore, we have chosen to develop a continuum model separately for EW and LW. EW is softer and absorbs most of the energy during refining, while LW is stiff and easily remains underdeveloped (Hickey and Rudie 1993). A combination of experimental work and numerical analysis has previously been used by Brabec et al. (2015) and Milch et al. (2016) to study wood compression behaviour, while dry wood and longitudinal compresion were in focus in the context of wood constructions.

This paper is the result of an international joint effort to model the compression behaviour of Norway spruce, with the expertise of pre-fatigue treatment at VTT Technical Research Centre of Finland, quasi-static material compression testing at Aalto University (Finland), high strain rate compression test of wood at Mid-Sweden University (Sweden) and high speed imaging and image processing at Tampere University of Technology (Finland). In this paper, the quasi static and dynamic material testing is presented and the latter is introduced in the experimental part. The experimental design and the structure of the Voigt-Kelvin material model are introduced in Figure 1. The material model is introduced in more detail in the materials and methods section. The ultimate goal of this modelling study is to enable computer simulations of complete defibration actions aiming at the virtual optimization of the process. Because of the viscoelasticity of wood, the mechanical energy applied will partly always be dissipated into heat energy. The main challenge is then to design a mechanical process for fatigue development, which is causing a minimum of energy dissipation into heat.

Materials and methods

Raw material: Fresh Norway spruce was collected from roughly 80-year-old trees from Myrskylä in southern Finland. The sapwood

Authenticated | carolina.moilanen@tut.fi author's copy
Download Date | 4/8/17 5:58 AM

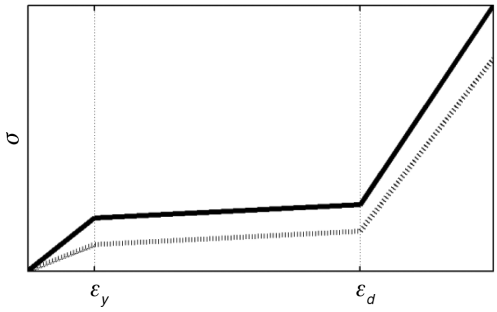

Figure 3: Simplified stress-strain curve for QSCT (dotted line) and HSRT (solid line), where ε_y denotes the yield limit and ε_d denotes densification limit.

samples were free from defects and stored in a freezer. Sample size for quasi static compression tests (QSCT) was 5×5×5 mm³, while that for high strain rate testing (HSRT) was 6 (R)×12×12 mm³. The raw material and testing equipment are presented in Figure 2. The MC of the samples was ca. 30%. This was measured by comparing the density of the sample to that of an oven dry sample. All samples were adjusted with a microtome to get parallel loading surfaces and a clear surface for the image based measurement. Some samples were pre-fatigued by 20 000 strain pulses delivered at 500 Hz in a device described by Lucander et al. (2009) and Salmi et al. (2009). This fatigue treatment can be considered intensive as the surface compression double amplitude was 1.0 mm. Four samples were tested at each temperature and strain rate for both native wood (W) and fatigued wood (W_{fat}). One $W_{fat,100°C}$ after HSRT could not be successfully analysed and therefore, results from only three samples are presented. Additionally, one native sample was subjected to cyclic QSCT.

Material testing: The material model developed here takes the strain rate into account and required material testing at two different strain rates, QSCT with a strain rate of ca. 0.004 s^{-1} and HSRT with global stain rates of 800 s^{-1} and 2400 s^{-1} (lower strain rate at high temperature). The QSCT was conducted in an Instron E1000 tensile testing machine (Instron, Norwood, MA, USA). At room temperature (rT), the wood samples were tested in air and in water submerged state at 80°C to prevent drying. The QSCT data at 80°C are compared to those of HSRT at 100°C.

The split-Hopkinson pressure bar (Mid-Sweden University, Sundsvall, Sweden) was used for HSRT, as usual, which was encapsulated in a thermally insulated pressure vessel (see Holmgren et al. 2008). The device was heated by saturated steam to 100°C for the high T samples. Details of this technique are already well described (Gray III 2000; Gray III and Blumenthal 2000; Widehammar 2002). The stress was calculated from the strain registered by strain gauges during HSRT, while the stress was measured with a load cell in the QSCT.

The local strain on fibre level was registered on an Infinity K2 long distance microscope (INFINITY PHOTO-OPTICAL GmbH, Göttingen, Germany) mounted on an Imperx Lynx GigE (IMPERX, Boca Raton, FL, USA) camera for the QSCT and on a Photron SA5 high speed camera (Photron, San Diego, CA, USA) for the HSRT. A frame rate of 2 Hz was applied during the QSCT, while the HSRT required a frame rate of 50 000–1 00 000 Hz. The resolution was 2.9–4.0 µm $pixel^{-1}$ for the HRST images and 2.1 µm $pixel^{-1}$ for the QSCT images. An image-based method according to Moilanen et al. (2015) was applied to analyse EW and LW compression. The interrogation area was 32×32 pixels for the QSCT images and 16×16 for the HSRT images. The image correlation was less accurate for the water submerged samples due to the reduced image contrasts. The free water in the lumen decreases the opacity of the surface, which leads to reflected light from varying surface depths.

Dynamic wood compression model: The compression rate affects the response of wood significantly. The expected difference between QSCT and HSRT compression is illustrated in Figure 3. In this example, the two samples have the same yield limit (ε_y) and densification limit (ε_d) but the MOE (in the formulae E_e) and the densification modulus (E_d) differ. The biggest difference for W_{sat} is in the elastic part of the stress-strain curve (Widehammar 2004).

A simple three part linear model was presented (Moilanen et al. 2016) to describe the EW compression, which did not take the strain rate explicitly into account, i.e. the model was only accurate at the strain rate of the experiments. It was assumed that wood behaves like a Voigt-Kelvin solid, in which the stress is a sum of the proportional parts to the strain and to the strain rate (Kolsky 1963). The second one represents the internal friction, i.e. the viscous effects. This model was modified in the present paper by adding the term $\eta\dot{\varepsilon}$ that is assumed to be linearly proportional to the strain rate (Equation 1):

$$\sigma_{EW} = \begin{cases} E_e^{EW}\varepsilon_{EW} + \eta^{EW}\dot{\varepsilon}_{EW} & \varepsilon_{EW} \le \varepsilon_y^{EW} \\ E_e^{EW}\varepsilon_y^{EW} + \eta^{EW}\dot{\varepsilon}_{EW} + E_p^{EW}\left(\varepsilon_{EW} - \varepsilon_y^{EW}\right) & \varepsilon_y^{EW} < \varepsilon_{EW} \le \varepsilon_d^{EW} \\ E_e^{EW}\varepsilon_y^{EW} + \eta^{EW}\dot{\varepsilon}_{EW} + E_p^{EW}\left(\varepsilon_d^{EW} - \varepsilon_y^{EW}\right) + E_d^{EW}\left(\varepsilon_{EW} - \varepsilon_d^{EW}\right) & \varepsilon_{EW} > \varepsilon_d^{EW} \end{cases} \quad (1)$$

where, the indices EW are for earlywood, i.e. σ_{EW} is the stress, E_e^{EW} is the MOE, E_p^{EW} is the plateau modulus, E_d^{EW} is the densification modulus, ε_y^{EW} is the yield limit, ε_d^{EW} is the densification limit and η^{EW} is the dynamic parameter. The variables in the model are the strain rate $\dot{\varepsilon}_{EW}$ and the strain ε_{EW}. The internal friction could be slightly different in the elastic and plastic regions as the mechanism of the compression changes, however, the viscous effect was modelled here as one single step to keep the model simple.

The LW compression can be assumed to be linear elastic, as it was described by Moilanen et al. (2016). In order to take the strain rate into account, a similar term $\eta\dot{\varepsilon}$ was added as in Equation 1,

$$\sigma_{LW} = E_e^{LW}\varepsilon_{LW} + \eta^{LW}\dot{\varepsilon}_{LW} \quad (2)$$

where the indices LW refer to latewood, i.e. σ_{LW} is the stress, E_e^{LW} is the MOE, η^{LW} is the dynamic parameter, $\dot{\varepsilon}_{LW}$ the strain rate, and ε_{LW} is the strain.

The parameters E_e^{EW}, E_p^{EW}, E_d^{EW}, ε_y^{EW}, ε_d^{EW} and E_e^{LW} are not strain rate dependent and were therefore fitted from the quasi static tests first, where the strain rate was practically zero (the compression in HRST was 800 s^{-1} and 2400 s^{-1}, while the QSCT strain rate was 0.004 s^{-1}). The parameters $\eta^{EW}$and η^{LW} were then used to fit the model to the HSRT data. The strain rate used was the local one, i.e. strain rates in EW or LW. The material parameters are dependent on both temperature and fatigue state. The parameter optimization was made for all parallel samples simultaneously with the least square method in MATLAB (MathWorks, Natick, MA, USA) (lsqcurvefit).

Authenticated | carolina.moilanen@tut.fi author's copy
Download Date | 4/8/17 5:58 AM

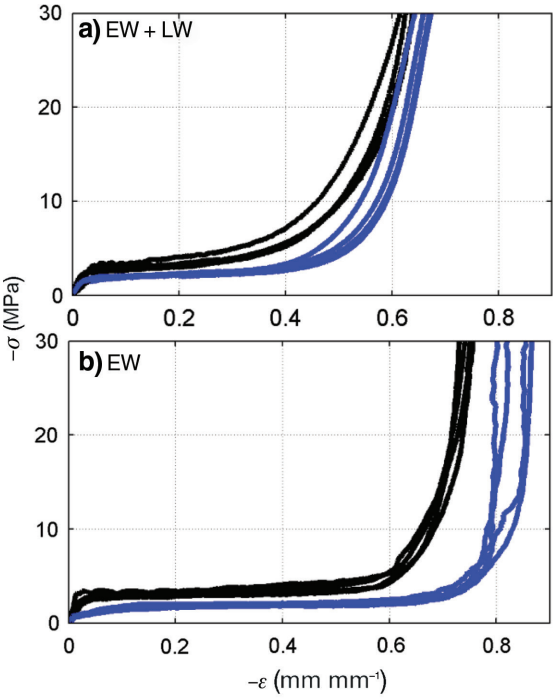

Figure 4: (a) Global stress-strain curves and (b) EW stress-strain curves for native samples tested in air (black solid line) and submerged in water (blue solid line) at rT.

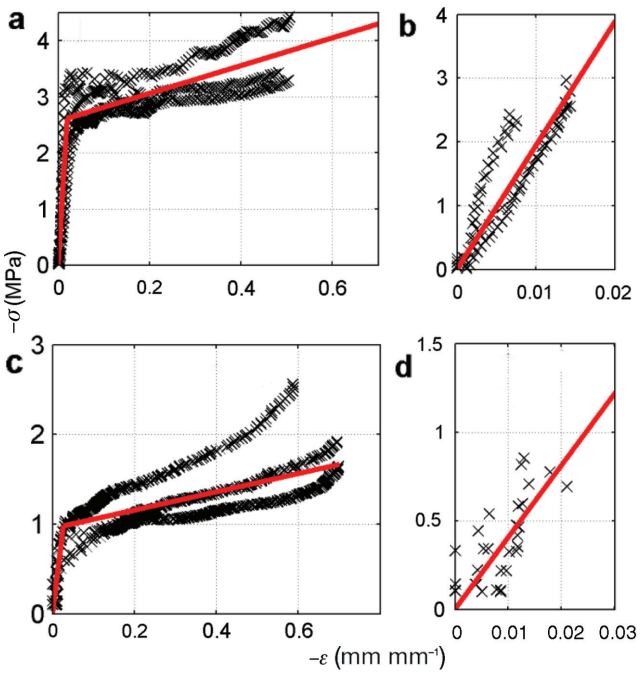

Figure 5: Stress-strain curves based on the QSCT model (red solid line) and experimental data (x) from compression tests of native (a) EW at rT, (b) LW at rT, (c) EW at $T_{80–100°C}$ and (d) LW at $T_{80–100°C}$.

The optimization could also be done separately for each sample and finally take the average of the parameters. It was shown by Moilanen et al. (2016) that the simultaneous optimization is preferable for the number of parallel samples used.

Results and discussion

The wood samples were submerged in a hot water (W_{H2O}) bath during the QSCT. At rT, both W_{H2O} and wood in air (W_{air}) were tested. The global stress-strain curves for native samples W_{air} and W_{H2O} are compared in Figure 4a and the EW stress-strain curves are presented in Figure 4b. The W_{H2O} is slightly softer than the W_{air} samples. The difference is more distinct in the EW stress-strain curves (Figure 4b) than in the global stress-strain curves (Figure 4a). The difference is assumed to be less significant at $T_{80–100°C}$, when temperature begins to dominate the softening. The $W_{QSCT, H2O}$ were treated at 80°C for safety reasons, while the HSRT device was heated with steam to 100°C. The softening of wood between 80°C and 100°C is low and significant softening occurs above 150°C (Salmén et al. 1997). Thus, the water softening will reduce the effect of the lower temperature in QSCT compared to the HSRT, but it is unknown how close is the actual QSCT behaviour of wood to that of wood with 30% MC at 100°C.

Compression model with static and dynamic terms for native wood

The densification region was not reached in the HSRT, therefore the material model was reduced to a two part linear model with the material parameters E_e^{EW}, E_p^{EW}, ε_y^{EW}, E_e^{LW}, η^{EW} and η^{LW}. The densification region was reached during the QSCT, but the stress-strain curves were cut off after the plateau region in the analysis in Figure 5 because the densification region was not included in the dynamic model.

The model for native wood is compared to test results in Figures 5 and 6. The model is fitted for four parallel samples and these are presented in Figure 5 (QSCT model) but only one of each is shown in Figure 6 (HSRT). The QSCT model in Figure 6 highlights the effect of the dynamic parameter. The strain rate was not constant in the HSRT, which causes the dynamic model to fluctuate. Figure 5a and b are the QSCT model for native EW (Figure 5a) and LW (Figure 5b) at rT, while Figure 5c and d are for native EW (Figure 5c) and LW (Figure 5d) at $T_{80°C}$. Figure 6a and b are similarly for native EW (Figure 6a) and LW (Figure 6b) at rT and Figure 6c and d for native EW (Figure 6c) and LW (Figure 6d) at $T_{100°C}$. The QSCT model curve overlaps the dynamic model curve in Figure 6d, which is therefore hard to see. Note that the scales of the strain

Authenticated | carolina.moilanen@tut.fi author's copy
Download Date | 4/8/17 5:58 AM

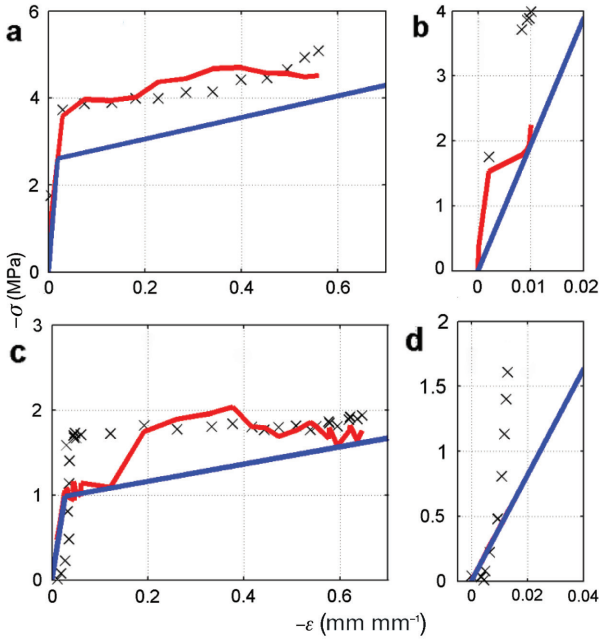

Figure 6: Stress-strain curves based on the dynamic model (red solid line), the QSCTc model (blue solid line) and experimental data (x) for four native samples tested at high strain rate (a) EW at rT, (b) LW at rT, (c) EW at $T_{80-100°C}$ and (d) LW at $T_{80-100°C}$.

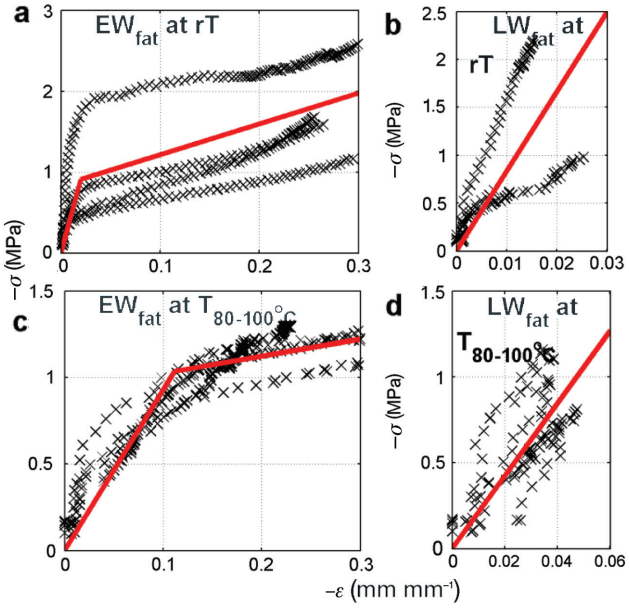

Figure 7: Stress-strain curves based on the QSCT model for fatigued wood (W_{fat}, red solid line) and experimental data (x) from compression tests of (a) EW at rT, (b) LW at rT, (c) EW at $T_{80-100°C}$, and (d) LW at $T_{80-100°C}$.

axes are different in the LW and EW stress-strain curves. The yield limit for native EW did not change significantly as a function of temperature. This was previously seen for averaged wood (EW + LW) by Uhmeier et al. (1998). This is because the yield limit depends mainly on the geometry of the wood material, which does not change with T.

Compression model with static and dynamic terms for fatigued wood

The compression model was also fitted to data from pre-fatigued samples (W_{fat}). Moilanen et al. (2016) modelled the compression behaviour of W_{fat} with an additional region before the yield limit (where the treated fibres collapse). Here, the model for W_{fat} has the same structure as that of native wood (W) including an initial linear elastic region up to the yield limit and thereafter a plateau region. This approach simplifies material modelling and later the model utilisation, especially the transition from W to W_{fat}.

Stress-strain curves of W_{fat} based on the QSCT model and on experimental data are presented in Figure 7, Figure 7a and b are for EW_{fat} (Figure 7a) and LW_{fat} (Figure 7b) at rT and Figure 7c and d for EW_{fat} (Figure 7c) and LW_{fat} (Figure 7d) at $T_{80°C}$. In Figure 8, the HSRT curves for W_{fat} based on the dynamic model are presented; Figure 8a and b are for EW_{fat} (Figure 8a) and LW_{fat} (Figure 8b) at rT, while Figure 8c and d are for EW_{fat} (Figure 8c) and LW_{fat} (Figure 8d) at $T_{80-100°C}$. The model fitted based on the QSCT model is included in Figure 8 for comparison. The QSCT model curve overlaps the dynamic model curve in Figure 8c, which is therefore hard to see.

Material model parameters

The compression model was fitted so that the material parameters E_e^{EW}, E_p^{EW}, ε_y^{EW} and E_e^{LW} are fitted from QSCT data and η^{EW} and η^{LW} are optimized from the HSRT data. The difference between the QSCT model and the dynamic model is the addition of the term $\eta\dot{\varepsilon}$, where $\dot{\varepsilon}$ is the strain rate in EW or LW from the corresponding test. The reason why the dynamic model fluctuates is the variations in the local strain rate. The material parameters are summarised in Table 1.

The yield limit for EW_{fat} tested at rT was surprisingly lower than that for native EW. The difference was however quite small and was likely due to the natural variation of the wood material. Another possibility is that the wood had not recovered completely and therefore had some residual strain remaining from the fatigue treatment. At high temperature, the yield limit of EW_{fat} was significantly larger. The elastic moduli for EW_{fat} and LW_{fat} were significantly smaller than for W both at rT and $T_{80-100°C}$.

Authenticated | carolina.moilanen@tut.fi author's copy
Download Date | 4/8/17 5:58 AM

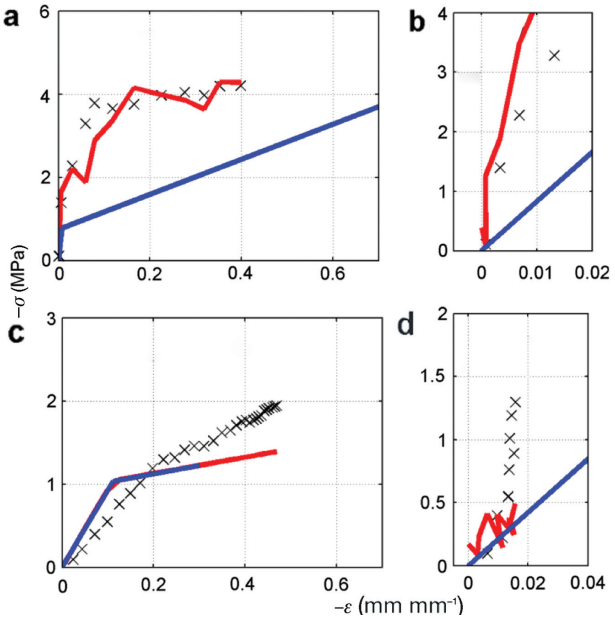

Figure 8: Stress-strain curves based on the dynamic model (red solid line), the quasi static model (blue solid line) and experimental data (x) for four fatigued samples tested at high strain rate (a) EW at rT, (b) LW at rT, (c) EW at $T_{80–100°C}$ and (d) LW at $T_{80–100°C}$.

Table 1: Summary of earlywood (EW) and latewood (LW) material parameters and 95% confidence intervals (CI) for native wood (W) and fatigued wood (W_{fat}).

Material	ε_y^{EW} –	E_e^{EW} MPa	E_p^{EW} MPa	η^{EW} MPa·s	E_e^{LW} MPa	η^{LW} MPa·s
W at rT	−0.019	133.9	2.5	$3.9 \cdot 10^{-4}$	194.0	$1.9 \cdot 10^{-3}$
CI, low	−0.021	124.6	2.2	$3.3 \cdot 10^{-4}$	181.6	$1.6 \cdot 10^{-3}$
CI, high	−0.018	143.3	2.7	$4.6 \cdot 10^{-4}$	206.4	$2.2 \cdot 10^{-3}$
W_{fat} at rT	−0.008	99.6	4.1	$8.3 \cdot 10^{-4}$	83.0	$1.9 \cdot 10^{-3}$
CI, low	−0.012	53.9	3.4	$7.4 \cdot 10^{-4}$	72.7	$1.7 \cdot 10^{-3}$
CI, high	−0.004	145.3	4.8	$9.2 \cdot 10^{-4}$	93.4	$2.0 \cdot 10^{-3}$
W at $T_{80–100°C}$	−0.027	36.2	1.0	$1.0 \cdot 10^{-4}$	40.7	$8.3 \cdot 10^{-4}$
CI, low	−0.032	30.3	0.9	$7.4 \cdot 10^{-5}$	34.2	$5.4 \cdot 10^{-4}$
CI, high	−0.023	42.1	1.1	$1.3 \cdot 10^{-4}$	47.2	$1.1 \cdot 10^{-3}$
W_{fat} at $T_{80–100°C}$	−0.112	9.3	1.0	$1.2 \cdot 10^{-6}$	21.1	$6.2 \cdot 10^{-4}$
CI, low	−0.116	9.0	0.9	$-3.2 \cdot 10^{-5}$	19.7	$5.0 \cdot 10^{-4}$
CI, high	−0.107	9.6	1.1	$3.5 \cdot 10^{-5}$	22.6	$7.5 \cdot 10^{-4}$

rT, room temperature; W_{fat}, wood after pre-fatigue treatment.

The plateau modulus was slightly higher for EW_{fat} than for native EW at rT but the same at high temperature. The parameters η^{EW} and η^{LW} were slightly higher for W_{fat} than for W at rT. Law et al. (2006) saw a drop of radial MOE by 84% when the temperature was increased from 22°C to 140°C. Here, the drop of MOE was 73% for native EW and 90% for EW_{fat}. Only a rough approximation of temperature and fatigue dependence can be determined, because only 2 temperatures and 2 fatigue states were measured. These trends are presented in Figure 9 with thinner lines representing the 95% confidence intervals.

The results in Figure 9a indicate that ε_y^{EW} increases more rapidly for fatigued wood than for native wood and that the values at rT are nearly the same. The difference in the MOE E_e^{EW} between W and W_{fat} appears to be constant with increasing T, which is demonstrated in Figure 9b. The effect of the fatigue treatment is reduced at increased T for both the plateau modulus E_p^{EW} (Figure 9c) and the parameter η^{EW} (Figure 9e). For LW, the results in Figure 9d indicate that the MOE E_e^{LW} decreases more rapidly at elevated T both for W than for W_{fat}. Figure 9f shows that the parameter η^{LW} is significantly reduced at higher T.

Cyclic compression test

The effect of low strain rate fatigue was investigated by advancing cyclic compressions with increasing maximum strain that was synchronised with images. The global stress-strain curve from the cyclic compressions of a native wood sample is presented in Figure 10a and the corresponding curve for image based EW strain is seen in Figure 10b. The numbers I–III in Figure 10 marks the

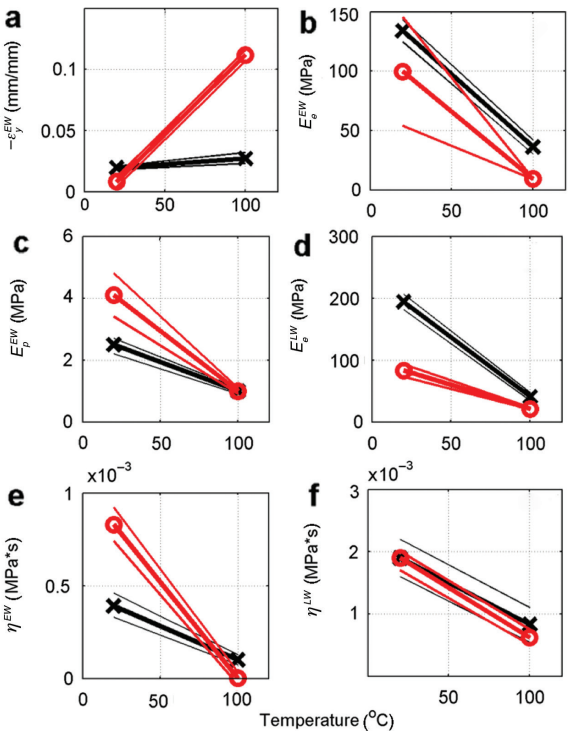

Figure 9: Earlywood material parameters. (a) ε_y^{EW}, (b) E_e^{EW}, (c) E_p^{EW} and (e) η^{EW} and latewood material parameters (d) E_e^{LW} and (f) η^{LW} for native wood (black solid line and x) and fatigued wood (red solid line and o) as a function of temperature with the 95% confidence intervals (thin solid lines).

Authenticated | carolina.moilanen@tut.fi author's copy
Download Date | 4/8/17 5:58 AM

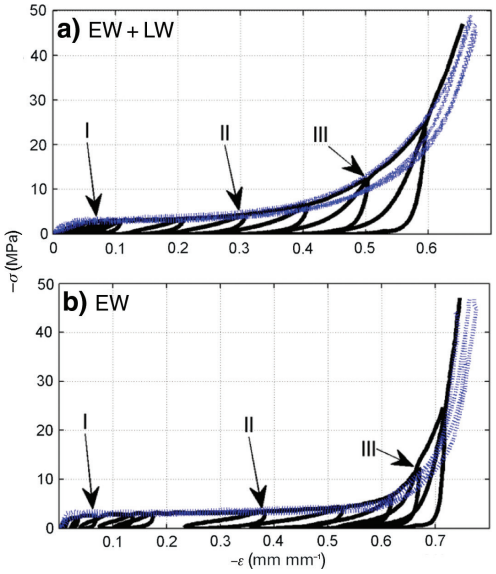

Figure 10: Stress-strain curves from quasi static cyclic loading of native wood (solid line) and single loading of native wood (blue dotted line) at rT (a) global strain, (b) image based earlywood strain, where the numbers I-III indicates the positions where the images in Figure 10 were captured.

positions during loading, where the images in Figure 11 were captured. The stress-strain curves from QSCT of single compression tests of W at rT are plotted with blue dotted lines in Figure 10 to emphasise that the upper part of the cyclic curve corresponds to that of W subjected to one single compression.

Figure 11a–c show two images captured at the same strain level during two consecutive compression cycles. The image to the left in Figure 11a is captured at maximum strain in the end of the 2nd compression cycle and the image to the right in the middle of the 3rd compression cycle at the same strain level. The images in Figure 11b are correspondingly captured in the end of the 6th compression cycle and in the middle of the 7th compression cycle and the images in Figure 11c are captured in the end of the 9th compression cycle and in the middle of the 10th compression cycle.

In the stress-strain curve of the advancing cyclic testing shown in Figure 10a, it is visible that the compressions move the yield limit $\left(\varepsilon_y^{EW}\right)$ to the right and reduce the MOE $\left(E_e^{EW}\right)$. After the maximum strain of the previous compression, the compression progresses as in native wood. Furthermore, from Figure 11 it is obvious that the cells have collapsed identically the second time if the compression reaches the same strain level. The image-based strain analysis for the cyclic test shows that the overall behaviour of EW was the same as for average wood that was registered by the testing equipment. However,

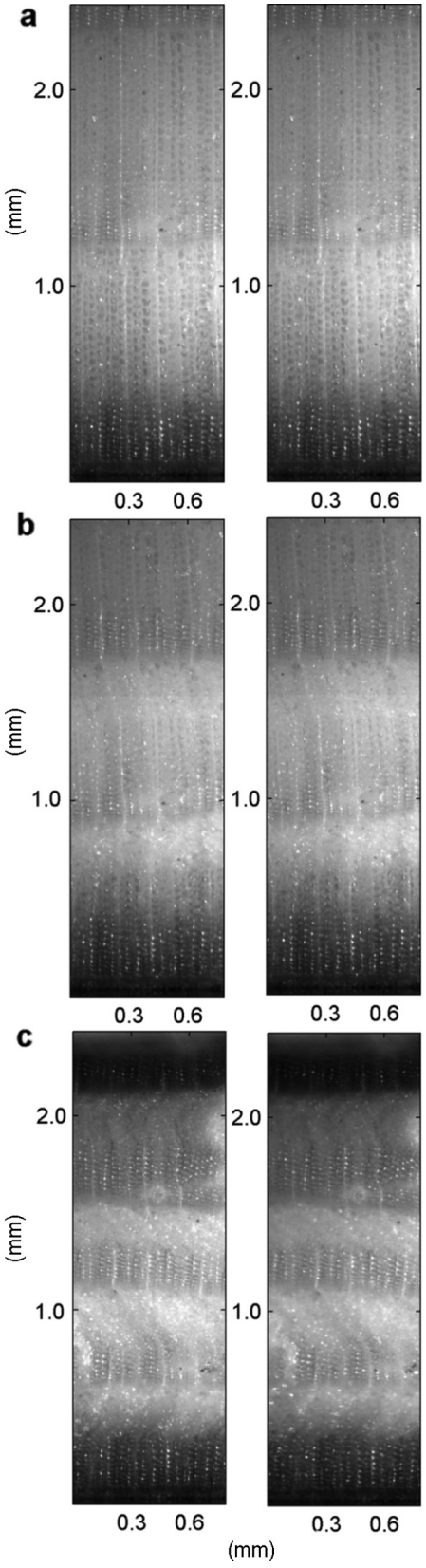

Figure 11: Images from the cyclic compressions captured at positions (a) I during the second and third compression cycles, (b) II during the sixth and seventh compression cycles and (c) III during the ninth and tenth compression cycles.

Authenticated | carolina.moilanen@tut.fi author's copy
Download Date | 4/8/17 5:58 AM

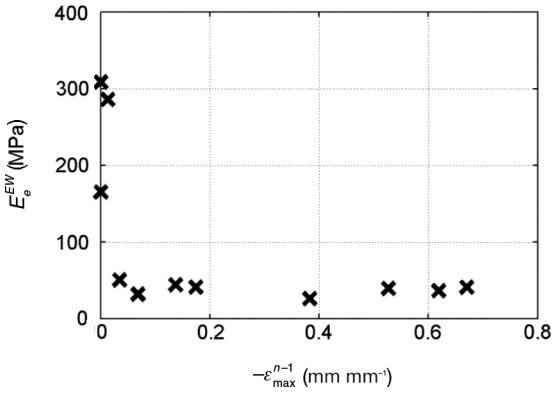

Figure 12: The elastic modulus E_e^{EW} as a function of maximum strain of the previous compression.

Figure 10b demonstrates that the relaxation of the samples was incomplete (the compression cycles do not return to zero). The piston was raised to the initial position after every compression but the sample did not have time to relax completely. The results from the cyclic EW compressions show how the wood was softened by each compression. The calculated value for the MOE $\left(E_e^{EW}\right)$ is plotted as a function of the maximum strain of the previous compression in Figure 12 for all compression cycles in Figure 10b.

The analysis behind the points in Figure 12 is based on the testing of one single sample and the uncertainty is therefore rather large. The image series was also significantly longer than the tests with one single compression, which can cause accumulation of measurement noise. The MOE of the compressions 2 and 3 are larger than the initial MOE, which was probably caused by an insufficient relaxation time. Figure 12 shows that the MOE was reduced immediately in the beginning of the compression cycle.

The measured MOE for W was slightly smaller than the initial MOE in Figure 12. This difference was probably caused by the natural large variation between different wood samples and the fact that only one sample was cyclically tested. The measured MOE of W_{fat} was higher than the final MOE in Figure 12. This difference indicates that the W_{fat} was not as fatigued as wood in the end of the cyclic experiment, even if the pre-fatigue treatment was intense. This is due to the fact that only the surface layer of the pre-fatigued sample was treated but the measured MOE is valid for the entire sample.

Conclusions

A dynamic wood compression model has been developed as parameters of a Voigt-Kelvin solid. The elastic effect is modelled by multiple regions using local strain in EW and LW, respectively. The viscous effect present at high strain rate is modelled by a strain rate dependant parameter also considering the local strain rate in EW and LW, respectively. The effect of fatigue treatment and temperature increase can be roughly seen in the material parameters for native wood (W) and fatigued wood (W_{fat}) measured at rT and at $T_{80–100°C}$. The strain rate dependent parameter for both EW and LW approaches zero at $T_{80–100°C}$. This means that the stress-strain behaviour is not strain rate dependant at high temperatures, not even at strain rate comparable to strain rates in mechanical pulping. The difference between W and W_{fat} is diminishing for four out of six parameters at high T, which suggests that temperature is dominant to pre-fatigue. The advancing cyclic compression experiment clearly showed that identically repeating strain does not increase fatigue, either as new collapse patterns on fibre level or as lowered MOE. The same experiment also indicates that enough large single compression strain pulses should be offered by defibration tools to reach high efficiency in internal fibrillation.

Energy efficient internal and external defibration is the final goal in mechanical pulping. Wood behaviour modelling at the strain and stress levels does not directly reveal the level of internal and external defibration. However, strain and stress development can be used to estimate these levels, e.g. drop in MOE can be connected to internal fibre defibration and fibre surface stress caused by defibration tool could be connected to external fibre defibration.

More work would be required to present the material parameters more accurately as functions of temperature and fatigue state. This entails HSRT and QSCT at additional temperatures and of additional pre-fatigue states. However, the presented dynamic compression model will be very useful for simulations of wood behaviour in the mechanical pulping process.

Acknowledgements: The Academy of Finland is acknowledged for the funding of the project Woodmat (decision number 140462), in which this research has been conducted. The Swedish Knowledge Foundation and the member companies of the E2MP-Research Profile at Mid Sweden University are also acknowledged for supporting this research. M. Ovaska, A. Miksic and M. Alava are supported by the Academy of Finland through its Centres of Excellence Program (2012–2017 under project no. 251748). The authors are also grateful for the assistance with the high strain rate material testing by Max Lundström and Staffan Nyström in the Mid Sweden University Material's Lab.

Authenticated | carolina.moilanen@tut.fi author's copy
Download Date | 4/8/17 5:58 AM

References

Adalian, C., Morlier, P. (2001) A model for the behaviour of wood under dynamic multiaxial compression. Compos. Sci. Technol. 61:403–408.

Becker, H., Höglund, H., Tistad, G. (1977) Frequency and temperature in chip refining. Paperi Puu. 59:123–126, 129–130.

Björkqvist, T. A design method for an efficient fatigue process in wood grinding – an analytical approach. Doctoral Thesis, Tampere University of Technology, Tampere, Finland, 2002.

Björkqvist, T., Lautala, P., Saharinen, E., Paulapuro, H., Koskenhely, K., Lönnberg, B. (1999) Behaviour of spruce sapwood in mechanical loading. J. Pulp Pap. Sci. 25:118–123.

Brabec, M., Tippner, J., Sebera, V., Milch, J., and Rademacher, P. (2015) Standard and non-standard behaviour of European beech and Norway spruce during compression. Holzforschung 69:1107–1116.

De Magistris, F. Wood fibre deformation in combined shear and compression. Doctoral Thesis, KTH Royal Institute of Technology, Stockholm, Sweden, 2005.

Fernando, D., Muhic, D., Engstrand, P., Daniel, G. (2011) Fundamental understanding of pulp property development under different thermomechanical pulp refining conditions as observed by a new Simons' staining method and SEM observation of the ultrastructure of fibre surfaces. Holzforschung 65:777–786.

Gray III, G.T. (2000) Classic split-Hopkinson pressure bar testing. In: Vol 8 Mechanical Testing and Evaluation, ASM Handbook. ASM International. pp. 462–476.

Gray III, G.T., Blumenthal, W.R. (2000) Split-Hopkinson pressure bar testing of soft materials. In: Mechanical Testing and Evaluation, Vol 8, ASM Handbook. ASM International. pp. 488–496.

Hamad, W.Y., Provan, J.W. (1995) Microstructural cumulative material degradation and fatigue-failure micromechanisms in wood-pulp fibres. Cellulose 2:159–177.

Hanhijärvi, A., Mackenzie-Helnwein, P. (2003) Computational analysis of quality reduction during drying of lumber due to irrecoverable deformation. Part I: Orthotropic viscoelastic-mechanosorptive-plastic material model for the transverse plane of wood. J. Eng. Mech. 129:996–1005.

Hickey, K.L., Rudie, A.W. (1993) Preferential Energy absorption by earlywood in cyclic compression of Loblolly pine. International Mechanical Pulping Conference June 15–17 Oslo, Norway: 81–86.

Holmgren, S., Svensson, B.A., Gradin, P.A., Lundberg, B. (2008) An encapsulated split Hopkinson pressure bar for testing of wood at elevated strain rate, temperature, and pressure. Exp. Tech. 32:44–50.

Höglund, H., Bäck, R., Falk, B. and Jackson, M. (1997): Thermopulp – A new energy-efficient mechanical pulping process. Pulp Paper Can. 98:82–89.

Isaksson, P., Gradin, P.A., Hellström, L.M. (2013) A numerical and experimental study regarding the influence of some process parameters on the damage state in wood chips. Holzforschung 67:691–696.

Kolsky, H. Stress Waves in Solids. Dover Publications Inc., New York, 1963.

Law, K.N., Kokta, B.V., Mao, C. (2006) Compression properties of wood and fibre failures. J. Pulp Pap. Sci. 32:224–230.

Lecourt, M., Meyer, V., Sigoillot, J.-C., Petit-Conil, M. (2010) Energy reduction of refining by cellulases. Holzforschung 64:441–446.

Li, X., Cai, Z., Horn, E., Winandy, J.E. (2011) Effect of oxalic acid pretreatment of wood chips on manufacturing medium-density fiberboard. Holzforschung 65:737–741.

Lucander, M., Asikainen, S., Pöhler, T., Saharinen, E., Björkqvist, T. (2009) Fatigue treatment of wood by high-frequency cyclic loading. J. Pulp Pap. Sci. 35:81–85.

Milch, J., Tippner, J., Sebera, V. and Brabec, M. (2016) Determination of the elasto-plastic material characteristics of Norway spruce and European beech wood by experimental and numerical analyses. Holzforschung 70:1081–1092.

Moilanen, C.S., Saarenrinne, P., Engberg, B.A., Björkqvist, T. (2015) Image based stress and strain measurement of wood in the split-Hopkinson pressure bar. Meas. Sci. Tech. 26:085206.

Moilanen, C.S., Björkqvist, T., Engberg, B.A., Salminen, L.I., Saarenrinne, P. (2016) High strain rate radial compression of Norway spruce earlywood and latewood. Cellulose 23:873–889.

Neimsuwan, T., Wang, S., Philip Ye, X. (2008) Effects of refining steam pressure on the properties of loblolly pine (*Pinus taeda* L.) fibers. Holzforschung 62:556–561.

Renaud, M., Rueff, M., Rocaboy, A.C. (1996) Mechanical behaviour of saturated wood under compression Part 2: Behaviour of wood at low rates of strain some effects of compression on wood structure. Wood Sci. Technol. 30:237–243.

Salmen, L. (1987) The Effect of the Frequency of a mechanical deformation on the fatigue of wood. J. Pulp. Pap. Sci. 13: 23–28.

Salmen, L., Tigerstrom, A., Fellers, C. (1985) Fatigue of wood - characterization of mechanical defibration. J. Pulp Pap. Sci. 11:68–73.

Salmén, L., Dumail, J.F., Uhmeier, A. (1997) Compression behaviour of wood in relation to mechanical pulping. International Mechanical Pulping Conference June 9–13, 1997, Stockholm, Sweden: 207–211.

Salmi, A., Salminen, L., Hæggström, E. (2009) Quantifying fatigue generated in high strain rate cyclic loading of Norway spruce. J. Appl. Phys. 106:104905

Salmi, A., Saharinen, E., Hæggström, E. (2011) Layer-like fatigue is induced during mechanical pulping. Cellulose 18: 1423–1432.

Salmi, A., Salminen, L.I., Lucander, M., Hæggström, E. (2012a) Significance of fatigue for mechanical defibration. Cellulose 19:575–579.

Uhmeier, A., Salmén, L. (1996) Influence of strain rate and temperature on the radial compression behavior of wet spruce. J. Eng. Mater. Technol. Trans. ASME 118:289–294.

Uhmeier, A., Morooka, T., Norimoto, M. (1998) Influence of thermal softening and degradation on the radial compression behavior of wet spruce. Holzforschung 52:77–81.

Widehammar, S. (2002) A method for dispersive split Hopkinson pressure bar analysis applied to high strain rate testing of spruce wood. Doctoral Thesis, Uppsala University, Uppsala, Sweden.

Widehammar, S. (2004) Stress-strain relationships for spruce wood: Influence of strain rate, moisture content and loading direction. Exp. Mech. 44:44–48.

Xing, C., Wang, S., Pharr, G.M., Groom, L.H. (2008) Effect of thermomechanical refining pressure on the properties of wood fibers as measured by nanoindentation and atomic force microscopy. Holzforschung 62:230–236.

Authenticated | carolina.moilanen@tut.fi author's copy
Download Date | 4/8/17 5:58 AM